https://ntrs.nasa.gov/search.jsp?R=20170009006 2019-04-30T04:13:20+00:00Z

Gravity Wave Spectra in the Lower Stratosphere Diagnosed from Project Loon Balloon Trajectories

M. R. Schoeberl[1], E. Jensen[2], A. Podglajen[3], L. Coy[4,5], C. Lodha[6], S. Candido[5], and R. Carver[5]

[1] Science and Technology Corporation, Columbia, MD, USA
[2] NASA Ames Research Center, Moffett Field, CA, USA
[3] Laboratoire de Météorologie Dynamique, CNRS-UMR8539, Institut Pierre Simon Laplace, École Normale Supérieure, École Polytechnique, Université Pierre et Marie Curie, Paris, France, 2Laboratoire de Météorologie Dynamique/IPSL, UPMC Univ Paris 06, CNRS, Palaiseau, France
[4] NASA Goddard Space Flight Center, Greenbelt, MD, USA
[5] SSAI, Lanham, MD, USA
[6] Project Loon, X, Mountain View, CA, USA
Corresponding Author: Mark Schoeberl (mark.schoeberl@mac.com)

Key Points:

- Project Loon super-pressure balloons provide unique information about lower stratospheric gravity waves.
- The wave energy spectrum roughly follows a -2 power law nearly everywhere.
- The amplitude of the temperature fluctuations with periods shorter than a day is higher than some previous estimates.

Abstract

Project Loon has been launching super-pressure balloons since January 2013 to provide worldwide Internet coverage. These balloons typically fly between 18-21 km and provide measurements of winds and pressure fluctuations in the lower stratosphere. We divide 1,560 Loon flights into 3,405 two-day segments for gravity wave analysis. We derive the kinetic energy spectrum from the horizontal balloon motion and estimate the temperature perturbation spectrum (proportional to the potential energy spectrum) from the pressure variations. We fit the temperature (and kinetic energy) data to the functional form $T'^2 = T'_o{}^2 (\omega/\omega_o)^\alpha$ where ω is the wave frequency, ω_o is daily frequency, T'_o is the base temperature amplitude and α is the slope. Both the kinetic energy and temperature spectra show -1.9±0.2 power-law dependence in the intrinsic frequency window 3 - 50 cycles/day. The temperature spectrum slope is weakly anti-correlated with the base temperature amplitude. We also find that the wave base temperature distribution is highly skewed. The average tropical modal temperature is 0.77 K. The highest amplitude waves occur over the mountainous regions, the tropics, and the high southern latitudes. Temperature amplitudes show little height variation over our 18-21 km domain. Our results are consistent with other limited super-pressure balloon analyses. The modal temperature is higher than the temperature currently used in Lagrangian model gravity wave parameterizations.

1. Introduction

Gravity waves play and important role in the flux of momentum into the upper atmosphere [Fritts and Alexander, 2003, and references therein]. More recently gravity waves have been recognized as a key component in cloud formation in the upper troposphere [Jensen and Pfister, 2004; Schoeberl et al., 2014] and the polar stratosphere [Alexander et al., 2013, Orr et al., 2015]. Our knowledge of these gravity wave fluctuations is limited, especially in the lower stratosphere and upper troposphere, thus any new information on the distribution and intensity of these waves is welcome. In this paper we report on the analysis of Loon super-pressure balloon data. The Loon data provides a new and extensive source of information on gravity waves in the lower stratosphere.

Analysis of gravity waves observed by super-pressure balloons is described in a number of papers [e. g. Hertzog and Vial, 2001; Vincent et al., 2007]. Boccara et al. [2008] and Podglajen et al. [2016] detail the current approach to Lagrangian analysis super-pressure balloon data. The Boccarra et al. approach has been applied to Strateole/Vorcore and Concordiasi balloon campaigns with the goal of assessing the upward momentum flux of gravity waves in the South Polar regions [Hertzog et al., 2008]. This super pressure balloon data has also been used to evaluate reanalyses fields [Podglajen et al, 2014; Friedrich et al., 2017] .

The particular focus of this work is not the momentum fluxes but the pressure (temperature) fluctuations produced by gravity waves in the lower stratosphere and their potential impact on cloud formation and stratospheric dehydration. Stratospheric dehydration occurs as air rising from the tropical upper troposphere into the stratosphere passes through the cold tropical tropopause layer [Fueglistaler et al., 2009]. Water vapor is removed through cloud formation and the sedimentation of ice crystals. Gravity wave temperature fluctuations fine-tune this process by further suppressing the minimum temperature [Kim and Alexander, 2015] and affecting the ice crystal number and particle size distribution [Jensen et al., 2012; Spichtinger and Krämer, 2013; Kärcher et al., 2014; Dinh et al., 2016; Jensen et al., 2016; Schoeberl et al., 2016].

In Lagrangian models of stratospheric dehydration, the high-frequency gravity wave temperature fluctuations are added to the reanalysis temperature field [Jensen and Pfister, 2004; Schoeberl et al., 2016] because these fluctuations are muted in the reanalysis fields. Thus Loon data will help us better determine how to parameterize gravity waves in the Lagrangian models. Although our primary interest is in tropical gravity measurements, most of the Loon data is extra-tropical, so we extend our data analysis to the extra-tropical regions.

2. Description of the Project Loon data

Project Loon, hereafter referred to as Loon, has an overall goal of providing worldwide Internet coverage using a network of long-duration super-pressure balloons. These balloons, floating between 17 and 21 km, can form a network linked to a ground-based telecom provider.

Increasing or decreasing the pressure inside the balloon can adjust the float altitude. Thus the Loon balloons can navigate by changing altitude into different wind regimes. Loon launches began in 2013 and continue to the present. Our database for this research consists of 1,664 flights of which 1,560 are long enough for analysis. These flights occurred from Jan 1, 2013 through Dec. 31, 2016. Loon balloons are not permitted to fly everywhere, but there is good coverage in the Southern Hemisphere mid-latitudes and partial coverage of the Northern Hemisphere mid-latitudes and the tropics. Loon measurements add significantly to the data provided by other super-pressure balloon experiments such as Concordiasi [Rabier et al., 2010].

Each balloon has a solar powered payload that includes a GPS position sensor, a pressure sensor, a surface pointing radiometer and balloon gas temperature sensor [Friedrich et al., 2017]. Data from these sensors are recorded at 1–2 minute intervals with occasional gaps due to telemetry failures. We restrict ourselves to the GPS position and pressure sensor data since the balloon gas temperature is a poor indicator of ambient temperature. Loon has provided an upper bound on the uncertainties of the sensors: 1.5 hPa for pressure, 10 m for GPS location. Loon winds are derived from the changes in position. The GPS uncertainty suggests an accuracy upper bound of 0.33m/s on the derived wind speed.

3. Analysis of the Loon Data

We restrict our analysis to the 18-21 km region that has the highest density of balloon data. We examine each balloon flight and discard very short flights or obviously bad data sets. We remove time gaps in the data, abutting data sets if possible. We next remove the pressure jumps associated with navigation, or data abutments. To remove the jumps, we take the time derivative of the balloon pressure altitude and screen for anomalously high derivatives. We then set the anomalous derivatives to zero and reconstruct the balloon pressure integrating the derivative forward in time. This approach effectively knits together the data stream, removing the jumps; however, it can create altitude biases in the data set if we believe that the gravity wave amplitudes vary significantly within our altitude domain. To test for this possibility, we have performed experiments with a narrowed vertical domain and repeated our analyses. We found our results show little variation with altitude within the narrowed vertical domains, consistent with other studies [e.g. Kim and Alexander, 2013]. Finally, each balloon flight is further subdivided into two day intervals – long enough to resolve the pressure fluctuation frequency at 1 cycle/day and higher. Any linear trend over the segment is removed, and the data is interpolated onto a regular time grid. We use each segment's average position to tag longitude, latitude and height of the segment. From 1,560 usable balloon flights, we have extracted 3,405 two-day segments that fit within the altitude domain 18-21 km.

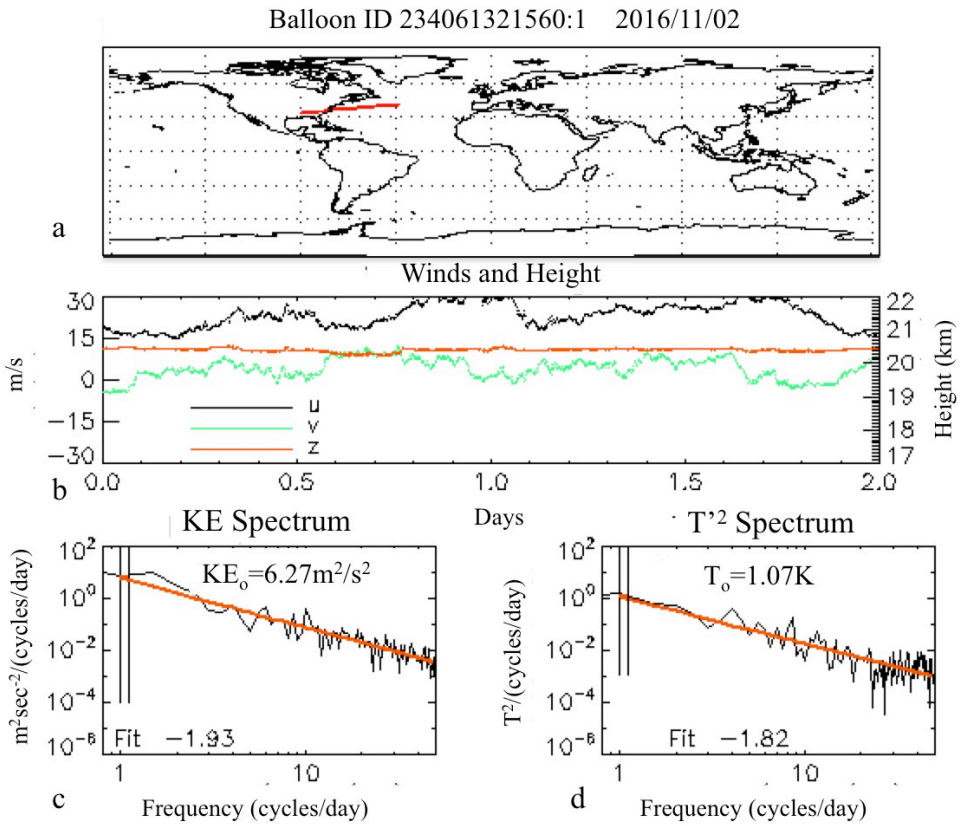

Figure 1. Sample analysis of a single balloon segment with the indicated flight date and ID. Top of figure (part a) shows the balloon flight path for this two-day flight segment. The middle plot (part b) shows the wind speed and log-pressure altitude of the balloon. Bottom plots show the *KE* (part c) and T'^2 (part d) spectrum, the 1 cycle/day value, and the fit derived from data between 3 cycles/day and 50 cycles/day. The vertical lines in the bottom figures show the averaging region used to generate KE_o and T'_o.

Figure 1 shows a sample of Loon data from a single segment. The figure shows the location of the balloon segment and the wind and log-pressure altitude z ($H \log_e(p_s/p)$, H is the scale height, ~7 km, p is pressure, p_s is a reference pressure, 1000 hPa). From this data we compute the Lagrangian kinetic energy and temperature power spectrum as shown in Figure 1. Our approach is identical to that used by Podglajen et al. [2016]. We assume that the balloon isopycnic perturbation vertical displacement, ζ'_B is related to the isentropic vertical displacement $\zeta'_B = \sigma\zeta'$ where σ is ~ 0.3 [Vincent and Hertzog, 2014; Podglajen et al., 2014]. Primes indicate perturbations from the mean. Next, we relate the isentropic vertical displacement to the

Lagrangian temperature fluctuations assuming (dry) adiabatic expansion, $T' = -\zeta' g / C_p$ where C_p is the specific heat of dry air at constant pressure, and g is the acceleration due to gravity.

The kinetic energy (KE) can be obtained from the horizontal velocities; the kinetic energy associated with vertical wind perturbations is much smaller and can be neglected. The potential energy E_p is related to the vertical displacement and hence the temperature perturbation, $E_P = \frac{1}{2}(C_P N / g)^2 T'^2$, where N is the buoyancy frequency. Instead of computing the potential energy, we focus on T'^2 since that is the relevant quantity for cloud dehydration. After computing the power spectrum as a function of frequency for KE and T'^2, we model the temperature and KE spectrum as $T'^2 = T'^2_o (\omega/\omega_o)^\alpha$ and $KE = KE_o(\omega / \omega_o)^\alpha$ where α is the fit for frequencies between 3 and 50 cycle/day and T'_o and KE_o are the value at frequency ω_o, 1 cycle/day. Fig. 1 shows an example of such a fit extended to 1 cycle/day from the 3-50 cycles/day fit. As shown by Massman [1978], Dinh et al., [2016], and Podglajen et al. [2016] inertial super-pressure balloon motions are at a much higher frequency than our fit region and therefore do not contaminate our results. The value of T'_o is determined by averaging the data between 1 and 1.1 cycles/day, shown as vertical bars in the figure, or T'_o can be determined from the 3 - 50 cycles/day fit by extrapolating the fit to 1 cycle/day. Both methods give nearly the same value. The α values (labeled Fit in the figure) are also shown.

4 Results

4.1 Spectrum slope and T'_o distributions

To get a good idea of the distribution of high frequency waves in the UTLS region we plot T'_o as a function of latitude-longitude (Figure 2a) and latitude-height (Figure 2b). Figures 3a and 3b shows the KE_o distribution. The highest concentration of Loon segments is in the Southern Hemisphere, and the largest values for T'_o and KE_o values are found over topography in both hemispheres (the Rockies and the Andes) and near the high southern latitudes near the roaring 40's. This result is consistent with other gravity wave measurements over steep topography by balloons, rockets and satellite (e. g. Alexander, 1998; Eckermann et al., 1999; Hertzog et al., 2008; Alexander et al., 2013, Orr et al., 2015), and we might expect enhanced gravity wave generation in the strong southern hemisphere jet [Fritts and. Nastrom, 1992].. The height distribution of T'_o and KE_o (Figures 2b, 3b) shows highest values in the Southern Hemisphere with scattered large values in the north and a few large anomalies in the tropics. In general the T'_o appears to be less noisy than the kinetic energy spectrum.

Analysis of the wave amplitudes with height (not shown) shows that the magnitude of the waves is roughly constant between 18.6 and 21 km.. Kim and Alexander [2013] analysis of tropical gravity wave variance showed that wave amplitudes increased by a factor of 3 from 14-18 km and then decreased only by 16% from 18-21 km. These results are consistent with our

assessment that the gravity wave amplitudes do not show much change with altitude in our analysis region.

Figure 4 shows the distribution of spectrum for slopes for T'^2. Most of the spectrum follows the -2 or slightly shallower even in regions of high amplitude waves seen in Figs 2 and 3. The correlation between T'_o and the spectrum slope is -0.38; in other words, weaker anomalies tend to have shallower slopes; the spectrum tends to be redder with stronger anomalies. Figure 5 shows the distribution of all spectrum fits. The T'^2 and *KE* fits are computed independently in our analysis; however, they have very similar distributions. This gives us confidence in our analysis since the kinetic and potential energy are related through the gravity wave polarization relations and should have similar slopes except where the frequency approaches either the buoyancy frequency (which is outside of our fit range) or the Coriolis frequency [Fritts and Alexander, 2003; Podglajen et al., 2016]. We note that the T'^2 mean slope is about -1.91± 0.2 (half-max) with a slope range between -1.3 and -2.5; the *KE* distribution shows similar behavior. The spread in slopes in Fig. 3 are likely due to uncertainties in the power spectrum fit. Hertzog and Vial [2001] analysis the Ecuador balloon campaign data also noted the ubiquitous -2 power law in the intrinsic *KE* spectrum. In fact, power law behavior in the high-frequency gravity wave spectral slope appears to be fairly universal (Fritts and VanZandt [1993] and references therein). . Most authors agree that the *KE* and E_p -2 power law behavior results from wave saturation – limitation of the wave amplitude due to instabilities [Dewan, 1994; Dewan et al., 1992; Smith et al., 1987].

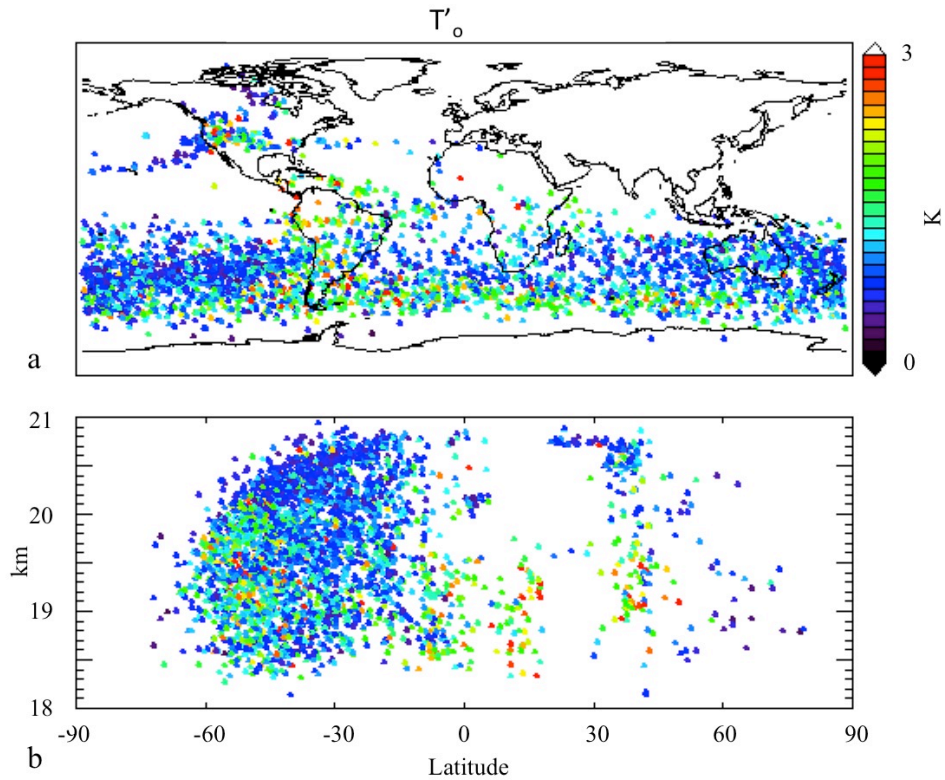

Figure 2. Distribution of T'_o values from individual two-day balloon segments. Part a shows the spatial distribution, while Part b shows the distribution with altitude.

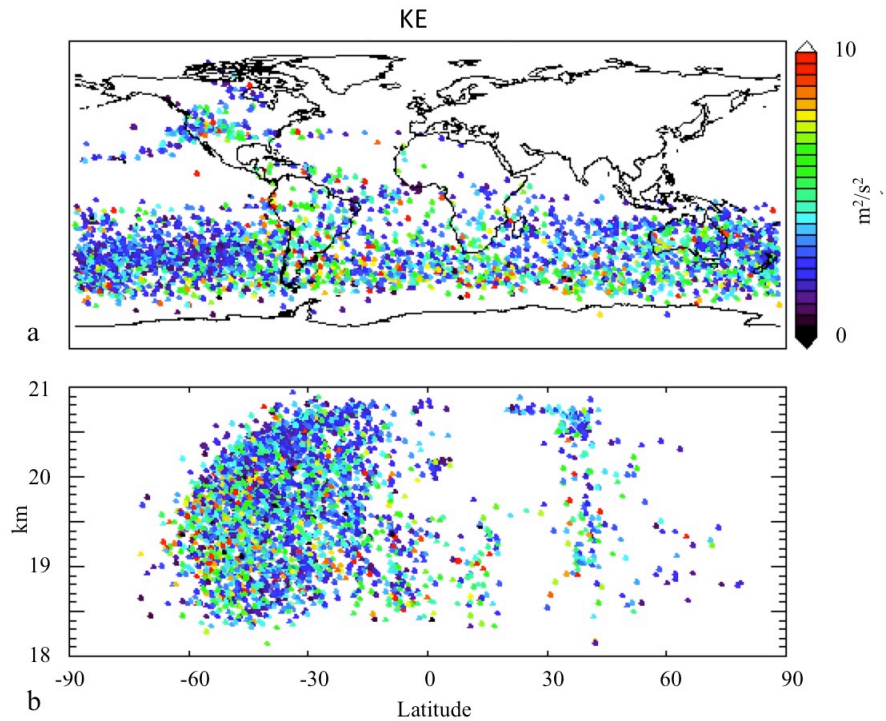

Figure 3. Distribution of T'_o values from individual two-day balloon segments. Part a shows the spatial distribution, while Part b shows the distribution with altitude.

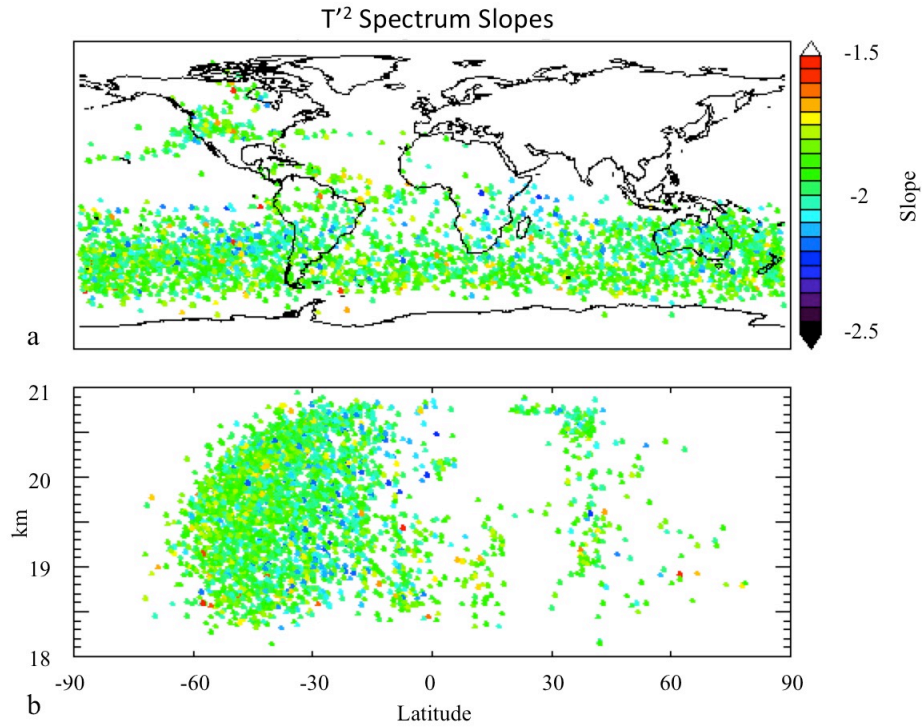

Figure 4. Distribution of T'^2 spectrum slopes from individual two-day balloon segments. Part a shows the spatial distribution, while Part b shows the distribution with altitude.

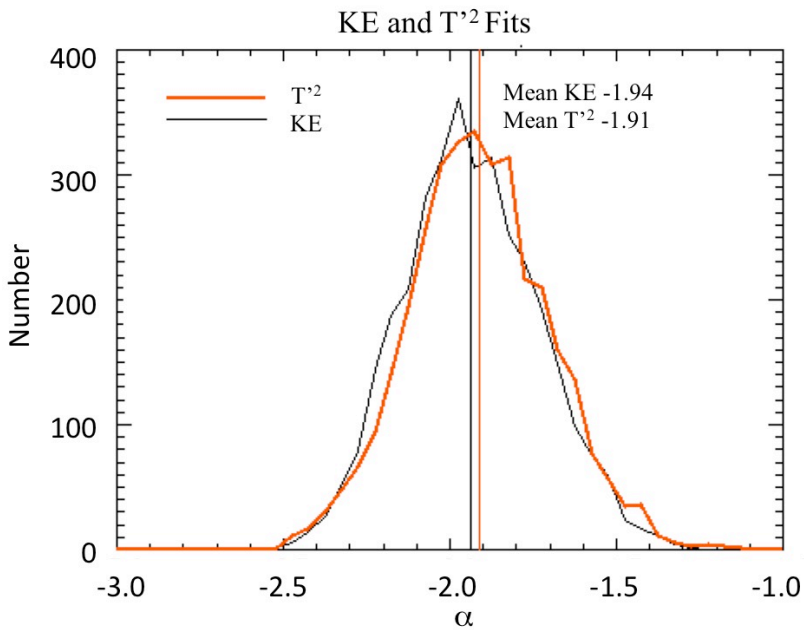

Figure 5. PDF of α values (slopes) for *KE* and T'^2 fits from all Loon 2-day segments. Mean values are the vertical lines.

Figure 6 shows T_o' distribution as a function of segment length. The distribution is quite skewed as previously observed for waves at very high southern latitudes [Baumgaertner and MacDonald , 2007; Alexander et al.,2015]. In other words, the mean is strongly weighted by the anomalous high amplitude events. The KE_o distribution (not shown) has a similar behavior. The mean and mode T'_o values are shown in the figure. The mode (0.77 to 0.45K) is ~ 0.3 K smaller than the mean; both the mean and the mode vary with segment length – increasing for shorter segments. The reason for the variation in mean and mode with segment length is that longer segments are composites of data from shorter segments and the compositing tends reduce the influence of the high amplitude events. Because the mode is the most frequent observed value, it makes sense to use the mode to characterize the wave amplitudes in models rather than the mean.

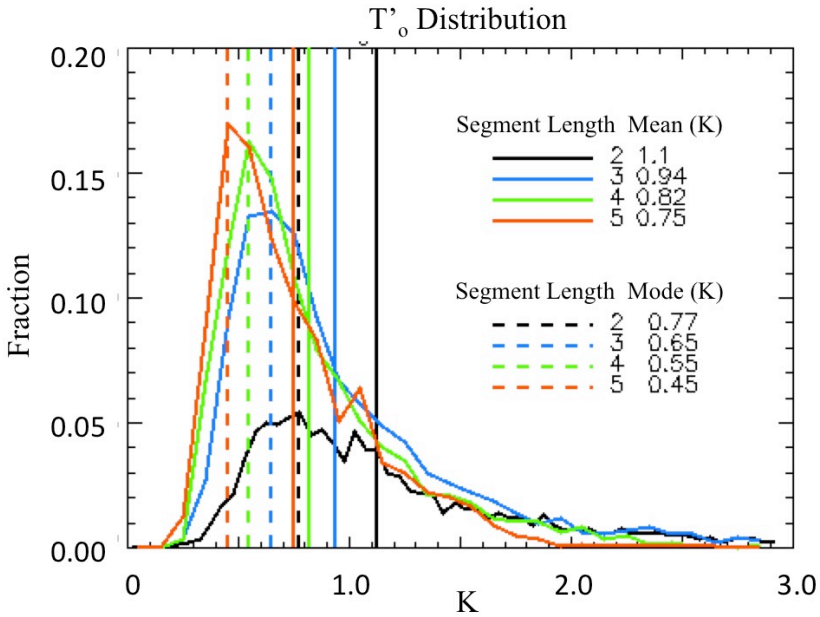

Figure 6. Normalized PDF of T'_o for all the Loon data using different segment lengths. The mean is shown with solid vertical lines and the mode with dashed lines. The caption shows the mean and mode values for different segment lengths: 2, 3, 4, and 5 days.

Seasonal variations in T'_o mean, mode and standard deviation values are shown in Figure 7. The usual seasonal divisions are used, DJF, MAM, JJA, SON. The data is grouped into 10º latitude zones and temperatures are binned by 0.1K to determine the mode. Means are shown as black dots and the mode is shown in red. Consistent with Fig. 6 the modal values are almost always below the mean value T'_o values. Gravity wave amplitudes are systematically higher over the southern hemisphere mid-latitudes with the exception of northern hemisphere winter. In JJA and SON tropical gravity wave values are high suggesting the influence of convection, but there is too little data to draw a definite conclusion. Overall, our seasonal variation is broadly consistent with the gravity wave climatology of Alexander [1998].

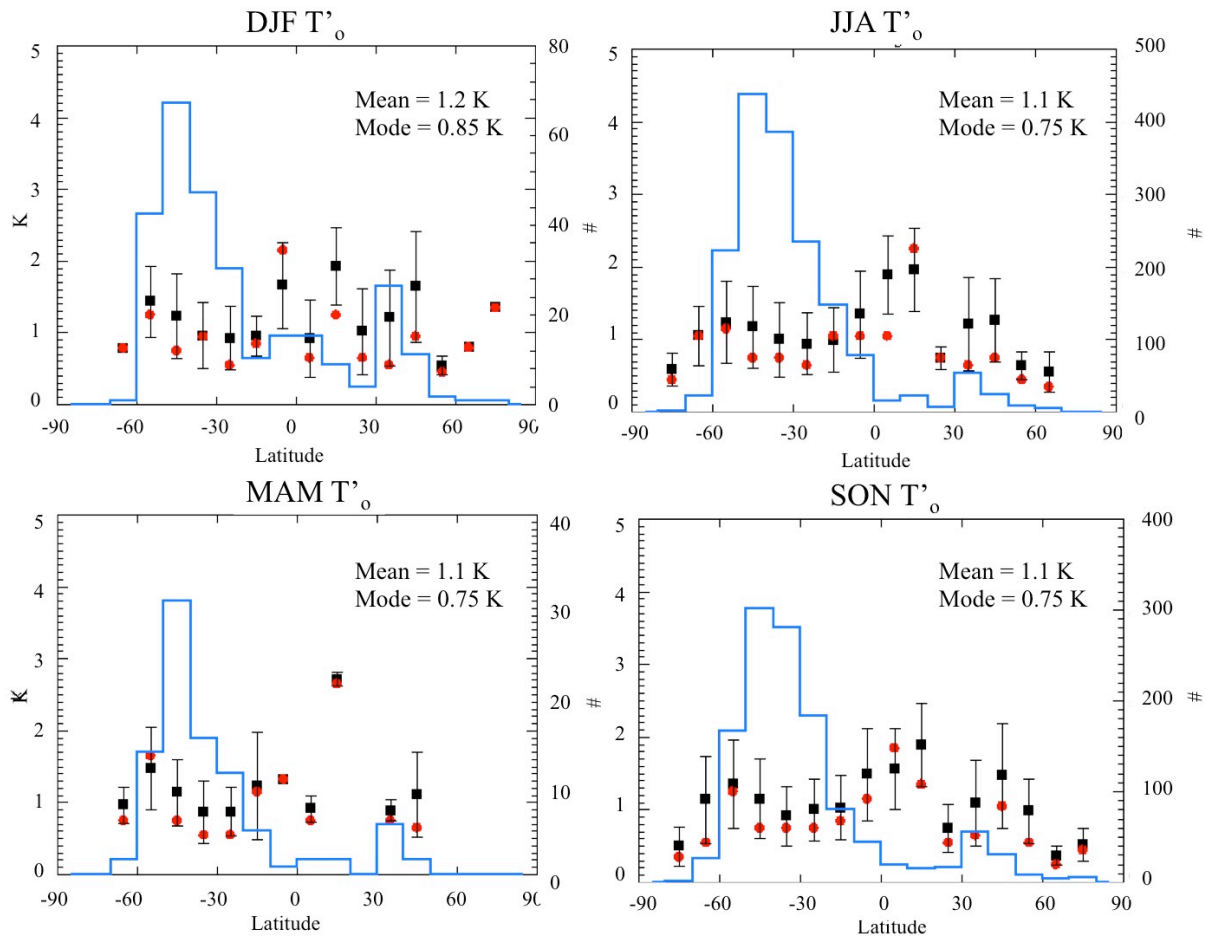

Figure 7. *T'$_o$* distribution as a function of latitude for the four seasons, DJF, MAM, JJA, SON as indicated in the titles. The points show the mean value with the vertical bars marking ± 1 standard deviation. Red dots show the modal values for each latitude bin. Blue lines indicate the number of measurements in each bin; number scale is shown on the right hand axis. The seasonal average mean and mode is shown in the upper right for each sub-figure.

4.2 Comparison with other estimates

Table 1 compares various estimates of the gravity wave temperature amplitudes in the lower stratosphere. As noted above, recent Lagrangian models of stratospheric dehydration [Jensen and Pfister, 2004; Ueyama et al. [2015]; Schoeberl et al., 2014, 2016] add high frequency gravity waves to the reanalysis fields (e.g. MERRA-2, Bosilovich et al., 2015; Molod et al., 2015). The reanalysis fields are available at 6-hour intervals, therefore the reanalysis cannot realistically represent high frequency waves. Computing the power spectrum of the wind and pressure fluctuations along a Lagrangian isentropic trajectory using MERRA and MERRA-2 data, we find lower *T'$_o$* values and a much steeper spectrum slope than indicated by our analysis of Loon data

(Table 1), which demonstrates the need to add the high frequency gravity waves to the reanalysis fields.

Kim and Alexander [2013, 2015] argued that gravity waves effectively suppress the temperature below the time averaged cold point. If the water vapor in the stratosphere is fixed at the coldest temperature an air parcel experiences when crossing the tropopause then 0.7 K reduction in temperature – about the size of the waves observed - would lower stratospheric water by ~ 0.5 ppmv, about 12% of the stratospheric average value; gravity waves are clearly important. Schoeberl et al. [2015], among others, argued that the cloud nucleation process complicates the gravity wave dehydration for high frequency waves so simply using the temperature suppression probably overestimates the effect on water vapor. In fact, as Schoeberl et al. [2016] show, high frequency waves play a more significant role in controlling tropical cirrus cloud fraction than in dehydration. Jensen et al. [2016] came to the same conclusion. Table 1 compares model values use by Jensen and Pfister [2004] (also used by Ueyama et al. [2015]) and Schoeberl et al. [2016]. The T'_o values used by those authors are much smaller than observations reported in this paper. Table 1 also shows that our assessment of the gravity wave amplitudes is in agreement with the analysis of the PreConcordiasi data by Podglajen et al. [2016]

5. Summary and Discussion

Project Loon has launched more than 1560 super-pressure balloons more or less continuously since 2013. These balloons float in the lower stratosphere between 18-21 km. We have analyzed the wind and pressure fluctuations that are part of the Project Loon tracking data. Each Loon flight is divided into two-day segments yielding 3,259 data sets. We have analyzed the *KE* and T'^2 spectrum for frequencies greater than 3 cycles/day and less 50 cycles/day following the approach of Podglajen et al. [2016]. We fit the data to the functional form $T'^2 = T_o'^2(\omega/\omega_o)^\alpha$ for both *KE* and T'^2. We find that α is -1.92± 0.2 for T'^2 and-1.94 ± 0.2 for *KE,* the spectrum slope roughly independent of latitude and altitude (Fig. 4), although there is a weak anti-correlation between the slope and the base amplitudes. Steeper slopes are associated with stronger anomalies; this is likely due to the fact the larger amplitude waves have not saturated so the high frequency components of the spectrum have not filled in. The T'_o and KE_o distributions are highly skewed, and it is probably best to use the modal amplitudes rather than the mean amplitude to represent typical wave amplitudes. Table 1 shows the data averaged modal and mean values for different regions.

The Loon data show higher wave amplitudes over topography, the Austral sub-polar regions and in the tropics (Figs. 2 and 3), which is consistent with many previous studies. Even though our analysis focuses on the lower stratosphere – just above the tropical tropopause - since we observe little variation in wave amplitude with height our results should be applicable to the tropical tropopause region. Below the tropical tropopause, the gravity wave amplitudes are expected to decrease at lower altitudes [Kim and Alexander, 2013].

Our results (Table 1) agree with the PreConcordiasi super-pressure balloon assessment of gravity wave amplitudes reported by Podglajen et al. [2016]. From our observations, Lagrangian models of stratospheric dehydration [Schoeberl et al., 2016, Ueyama et al., 2015] are adding too little high frequency gravity wave energy. Putting Loon values into the Schoeberl et al. [2016] model increases cirrus fraction by ~70 % compared to model results run with MERRA2 and no gravity waves. This puts the cloud fraction higher than the range of CALIOP observations. Jensen et al. [2016] used Pre-Concordiasi balloon measurements of temperature perturbations and found that homogeneous freezing driven by high-frequency waves produced higher ice concentrations than were observed in recent high-altitude aircraft campaigns. These two model results are broadly consistent. The discrepancy with observations can be resolved; however, if the amplitude of the gravity wave temperature spectrum (T_o) decreases at lower altitudes following the observations reported by Kim and Alexander [2013]. These studies will be reported in a publication currently in preparation.

Acknowledgments and Data

This work was supported under NASA grant NNX13AK25G and from the NASA Modeling, Analysis and Prediction program. Loon data is available from the Project Loon team, please contact lodha@x.team. MERRA-2 data can be downloaded from the NASA GES DISC (https://disc.gsfc.nasa.gov/datareleases/merra_2_data_release). We thank Joan Alexander for helpful comments on this manuscript. We would also like to thank one of the Reviewers (Adrian McDonald) for very helpful comments and suggestions.

References

Alexander, M. J. (1998), Interpretations of observed climatological patterns in stratospheric gravity wave variance, J. Geophys. Res., 103, 8627-8640.

Alexander, S. P., A. R. Klekociuk, A. J. McDonald, and M. C. Pitts (2013), Quantifying the role of orographic gravity waves on polar stratospheric cloud occurrence in the Antarctic and the Arctic J. Geophys. Res. Res., Atmos., 118, 11,493–11,507, doi:10.1002/2013JD020122

Baumgaertner, A. J. G. and A. J. McDonald (2007), A gravity wave climatology for Antarctica compiled from Challenging Minisatellite Payload/Global Positioning System (CHAMP/GPS) radio occultations, J. Geophys. Res., 112, D05103, doi:10.1029/2006JD007504

Boccara, G., Hertzog, A., Vincent, R. A., and Vial, F. (2008), Estimation of gravity-wave momentum fluxes and phase speeds from quasi-Lagrangian stratospheric balloon flights. Part I: Theory and simulations, J. Atmos. Sci., 65, 3042–3055, doi:10.1175/2008JAS2709.1

Bosilovich, M. G., and Coauthors, (2015), MERRA-2: Initial Evaluation of the Climate. NASA Tech. Rep. Series on Global Modeling and Data Assimilation, NASA/TM-2015-104606, Vol. 39, NASA, 136 pp.

Dewan, E. M., (1994), The saturated-cascade model for atmospheric gravity wave spectra, and the wavelength-period (W-P) relations, Geophys. Res. Lett., 21,817-820.

Dewan, E.M., Pendleton, W., Grossbard, N. and Espy, P. (1992), Mesospheric OH airglow temperature fluctuations: A spectral analysis, Geophys. Res. Lett., 19, 597-600.

Dinh, T. , A. Podglajen , A. Hertzog , B. Legras , and R. Plougonven (2016), Effect of gravity wave temperature fluctuations on homogeneous ice nucleation in the tropical tropopause layer Atmos. Chem. Phys., 16, 35–46, doi:10.5194/acp-16-35-2016.

Eckermann, S.D., P. Preusse (1999), Global measurements of stratospheric mountain waves from space. Science, 286, 1534–1537.

Fritts, D. C., and M. J. Alexander (2003), Gravity wave dynamics and effects in the middle atmosphere, Rev. Geophys., 41, 1003, doi:10.1029/2001RG000106.

Fritts, D. C., and G. D. Nastrom, (1992), Sources of mesoscale variability of gravity waves. Part II: Frontal, convective, and jet stream excitation. J. Atmos. Sci., 49, 111–127.

Friedrich, L. S., McDonald, A. J., Bodeker, G. E., Cooper, K. E., Lewis, J., and Paterson, A. J.: (2017), A comparison of Loon balloon observations and stratospheric reanalysis products, Atmos. Chem. Phys., 17, 855-866, doi:10.5194/acp-17-855-2017

Fueglistaler, S., A. E. Dessler, T. J. Dunkerton, I. Folkins, Q. Fu, and P. W. Mote (2009), The tropical tropopause layer, Rev. Geophys., 47, RG1004, 10.1029/2008RG000267.

Hertzog, A., and F. Vial (2001), A study of the dynamics of the equatorial lower stratosphere by use of ultra-long-duration balloons: 2. Gravity waves, J. Geophys. Res., 106(D19), 22,745–22,761, doi:10.1029/2000JD000242.

Hertzog, A., G. Boccara, R. A. Vincent, and F. Vial, (2008) Estimation of gravity-wave momentum fluxes and phase speeds from quasi-Lagrangian stratospheric balloon flights. Part II: Results from the Vorcore Campaign in Antarctica, J. Atmos. Sci., 65, 3056–3070, doi: http://dx.doi.org/10.1175/2008JAS2710.1

Jensen, E., and L. Pfister (2004), Transport and freeze-drying in the tropical tropopause layer, J. Geophys. Res., 109, D02207, doi:10.1029/ 2003JD004022.

Jensen, E. J., L. Pfister, and T. P. Bui (2012), Physical processes controlling ice concentrations in cold cirrus near the tropical tropopause, J. Geophys. Res., 117, D11205, doi:10.1029/2011JD017319.

Jensen, E. J., et al. (2016), High-frequency gravity waves and homogeneous ice nucleation in tropical tropopause layer cirrus, Geophys. Res. Lett.,43, doi:10.1002/2016GL069426.

Kärcher, B., J. Hendricks, and U. Lohmann (2006), Physically based parameterization of cirrus cloud formation for use in global atmospheric models, J. Geophys. Res., 111, D01205, doi:10.1029/2005JD006219.

Kärcher, B., A. Dörnbrack, and I. Sölch (2014), Supersaturation variability and cirrus ice crystal size distributions, J. Atmos. Sci., 71, 2905–2926,doi:10.1175/JAS-D-13-0404.1.

Kim, J.-E., and M. Joan Alexander (2013), A new wave scheme for trajectory simulations of stratospheric water vapor, Geophys. Res. Lett., 40, 5286–5290, doi:10.1002/grl.50963.

Kim, J.-E., and M. J. Alexander (2015), Direct impacts of waves on tropical cold point tropopause temperature, Geophys. Res. Lett., 42, 1584–1592, doi:10.1002/2014GL062737.

Massman, W. J. (1978), On the nature of vertical oscillations of constant volume balloons, J. Appl. Meteorol., 17, 1351–1356, doi:10.1175/1520-0450-1978

Molod, A., L. Takacs, M. Suarez, and J. Bacmeister, J. (2015) Development of the GEOS-5 atmospheric general circulation model: evolution from MERRA to MERRA2, Geosci. Model Dev., 8, 1339-1356, doi:10.5194/gmd-8-1339-2015.

Orr, A., Hosking, J. S., Hoffmann, L., Keeble, J., Dean, S. M., Roscoe, H. K., Abraham, N. L., Vosper, S., and Braesicke, P. (2015) Inclusion of mountain-wave-induced cooling for the formation of PSCs over the Antarctic Peninsula in a chemistry–climate model, Atmos. Chem. Phys., 15, 1071-1086, doi:10.5194/acp-15-1071-2015.

Podglajen, A., A. Hertzog, R. Plougonven, and N. Žagar (2014), Assessment of the accuracy of (re)analyses in the equatorial lower stratosphere, J. Geophys. Res. Atmos., 119, 11,166–11,188, doi:10.1002/2014JD021849.

Podglajen, A., A. Hertzog, R. Plougonven, and B. Legras (2016), Lagrangian temperature and vertical velocity fluctuations due to gravity waves in the lower stratosphere, Geophys. Res. Lett., 43, 3543–3553, doi:10.1002/2016GL068148.

Rabier, F., et al. (2010), The Concordiasi project in Antactica, Bull. Am. Meteorol. Soc., 91(1), 69–86, doi:10.1175/2009BAMS2764.1

Randel, W. J., and E. J. Jensen (2013), Physical processes in the tropical tropopause layer and their roles in a changing climate, Nat. Geosci. 6(3), 169–176, doi:10.1038/ngeo1733.

Schoeberl M. R., A. E. Dessler, T. Wang, M. A. Avery, and E. J. Jensen (2014), Cloud formation, convection, and stratospheric dehydration, Earth and Space Science, 1, 1–17, doi:10.1002/2014EA000014

Schoeberl, M. R., E. J. Jensen, and S. Woods (2015), Gravity waves amplify upper tropospheric dehydration by clouds, Earth and Space Science, 2, 485–500, doi:10.1002/2015EA000127.

Schoeberl, M., A. Dessler, H. Ye, T. Wang, M. Avery, and E. Jensen (2016), The impact of gravity waves and cloud nucleation threshold on stratospheric water and tropical tropospheric cloud fraction, Earth and Space Science, 3, doi:10.1002/2016EA000180.

Spichtinger, P., and M. Krämer (2013), Tropical tropopause ice clouds: A dynamic approach to the mystery of low crystal numbers, Atmos. Chem. Phys., 13(19), 9801–9818, doi:10.5194/acp-13-9801-2013.

Smith, S. A., Fritts, D. C. and Van Zandt, T. E. (1987) Evidence for a saturated spectrum of atmospheric gravity waves, J. Atmos. Sci., 44, 1404-1410.

Ueyama, R., E. J. Jensen, L. Pfister, and J.-E. Kim (2015), Dynamical, convective, and microphysical control on wintertime distributions of water vapor and clouds in the tropical tropopause layer, J. Geophys. Res. Atmos., 120, 10,483–10,500, doi:10.1002/2015JD023318.

Table 1. Comparison of base T'_o values at 1 cycle/day and the spectrum slope, α

Source	T'_o	α
MERRA Tropics (NH winter)	0.174	-3.61
MERRA-2 Tropics (NH winter)	0.17	-3.59
Jensen and Pfister [2004]	~ 0.4	-1.85
Schoeberl et al. [2016]	0.1	-2
Podglajen et al [2016]		
S. Pole	0.90	-1.78
Tropics	1.07	-1.96
Loon	Mean, Mode	
NH Mid Latitudes	1.22, 0.775	-1.89
SH Mid Latitudes	1.13, 0.625	-1.91
Tropics	1.23, 0.775	-1.88